Iranian Journal of Chemical Engineering

Full Length Article

Theoretical and Empirical Equilibrium Concentration for the Dry Reforming of Methane

Gh. Moradi *, H. Hemmati

Catalyst Research Center, Department of Chemical Engineering, Faculty of Engineering, Razi University, Kermanshah, Iran

ARTICLE INFO	ABSTRACT
	The Dry Reforming of Methane, which uses methane and carbon dioxide, the two greenhouse gasses, to produce synthesis gas, has received considerable attention recently. In this work, the equilibrium conversion that is the maximum possible conversion has been obtained experimentally and theoretically. The equilibrium concentration for the Dry Reforming of Methane (DRM) has been calculated using Thermodynamic equilibrium and compared with the experimental equilibrium concentration. The reaction coordinate (ε), Gibbs free energy (G), reaction equilibrium constant (K), and reaction stoichiometric coefficients are used for the calculation of the reaction progress and the equilibrium composition in DRM at different temperatures. These parameters have been calculated by two primary methods, direct and Lagrange, and compared with an empirical equilibrium that has been revealed by the activity test on Ni/Al$_2$O$_3$ catalyst. The result shows that none of those can't make an exact determination of empirical equilibrium compositions, but there was a relatively good agreement between the Lagrange method and the empirical equilibrium. No significant difference has been observed between these methods and empirical conditions at high temperature.

1. Introduction

The CO$_2$ reforming of methane has been one of the desirable reactions in this century. In this reaction, Methane and carbon dioxide as two inexpensive and greenhouse gases are involved but the product gas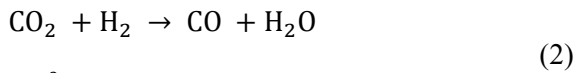 mixture (CO + H$_2$) which is produced is known as the most advantageous gas mixture to many refineries and petrochemical applications such as carboxylation, the hydrogenation of liquid hydrocarbon and Fischer–Tropsch, [1-3]. The main reaction of DRM is shown as follows [4]:

$$CH_4 + CO_2 \rightarrow 2H_2 + 2CO \qquad (1)$$

---
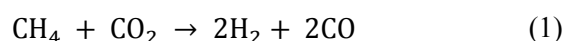
*Corresponding author: gmoradi@razi.ac.ir (Gh. Moradi)

$$\Delta H^0_{298} = 247 \text{ kJ/mol}$$

But this reaction isn't the only reaction that has occurred in DRM. The reverse water gas shift reaction (reaction No. 2) and the reverse of the Boudouard reaction (reaction No. 2) has also occurred in DRM [4, 5].
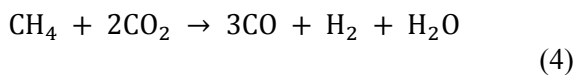
$$CO_2 + H_2 \rightarrow CO + H_2O$$
$$\Delta H^0_{298} = 39.5 \text{ kJ/mol} \qquad (2)$$

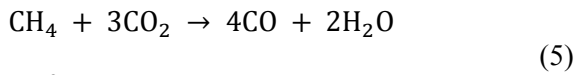$$2CO \rightarrow CO_2 + C$$
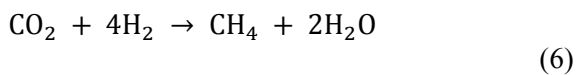$$\Delta H^0_{298} = -171 \text{ kJ /mol} \qquad (3)$$

Also, several side reactions (reaction No. 4-10) have occurred in the DRM reaction, and these reactions resulted in lowering the selectivity of products [5-8].
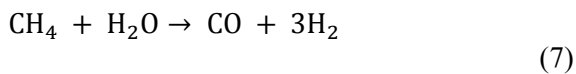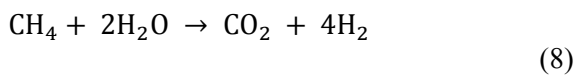
$$CH_4 + 2CO_2 \rightarrow 3CO + H_2 + H_2O$$
$$\Delta H^0_{298} = 228 \text{ kJ/mol} \qquad (4)$$

$$CH_4 + 3CO_2 \rightarrow 4CO + 2H_2O$$
$$\Delta H^0_{298} = 329 \text{ kJ/mol} \qquad (5)$$

$$CO_2 + 4H_2 \rightarrow CH_4 + 2H_2O$$
$$\Delta H^0_{298} = 165 \text{ kJ/mol} \qquad (6)$$

$$CH_4 + H_2O \rightarrow CO + 3H_2$$
$$\Delta H^0_{298} = 206 \text{ kJ/mol} \qquad (7)$$

$$CH_4 + 2H_2O \rightarrow CO_2 + 4H_2$$
$$\Delta H^0_{298} = 165 \text{ kJ/mol} \qquad (8)$$

$$CH_4 \rightarrow 2H_2 + C$$
$$\Delta H^0_{298} = 75 \text{ kJ /mol} \qquad (9)$$

$$CO + H_2 \rightarrow C + H_2O$$
$$\Delta H^0_{298} = -131.28 \text{ kJ /mol} \qquad (10)$$
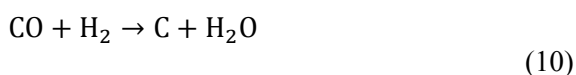
Many researchers studied the equilibrium

conditions of the ethanol reforming [8], steam and partial oxidation of natural gas [9, 10] and methane pyrolysis [8] using the direct method of Gibbs minimization, and the free energy with the software package [11]. Douvartzides et al. [9, 12] used the Lagrange method for calculating the thermodynamic equilibrium of the fuel cell, auto-thermal reforming of methane and methane combustion. Some researcher has calculated equilibrium compositions at many temperatures. Juan-Juan et al. estimated that the equilibrium conversion of methane was about 88 % at 973 K [8, 13]. Maier et al. suggested that at 873.15 K, the methane conversion was about 50 % and when the temperature was above 1023 K, the methane conversion was higher than 90 % [14]. But there are few researches on the calculation of empirical equilibrium compositions and comparing them with theoritical equilibrium compositions. The dry reforming of the methane reaction produces CO and H_2 as the main products of CH_4 and CO_2. CH_4 and CO_2 are chemically stable due to their high bond energy. Extreme temperatures are required to activate them and convert them to synthesis gas. Therefore, the study of the thermodynamics of the dry reforming of the methane reaction is useful for determining the thermodynamic limit of the process. In previous studies, various works have been done on the thermodynamic equilibrium of this process. A common feature of thoes studies is the Gibbs free energy minimization method. At temperatures below 550 °C, the resulting reaction mixture contains solid carbon (C_s) and H_2O along with CH_4 and CO_2. As the temperature rises, the reaction mixture is rich in synthesized gas. At 900 °C, the conversion of CH_4 and CO_2 can reach 98.1 % and 97.3 % respectively [4]. From a thermodynamic point of view, the solid carbon

formed by the side reactions, is practically negligible at this temperature. From the other hand, considering the stoichiometry of the main reforming reaction equation (1), it is obvious that low pressures and high temperatures are desirable for the dry reforming of the methane reaction [8].

As noted above, many reactions occurred in DRM, so it was tough to calculate equilibrium compositions and kinetics reaction. There are two ways for calculating the thermodynamics composition for the reaction. The first one, was using the reaction coordinate (ε) and reaction constant (K) for calculating the equilibrium composition and the other was using the Gibbs free energy and the minimization of this [15, 16]. There were two methods for the minimization of the Gibbs free energy, the direct method and the Lagrange multiplier method [15, 16].

Thermodynamic feasibility of the dry reforming process of methane shows that the conversion rates of methane and carbon dioxide increase by increasing the reaction temperature. In addition to the effect of temperature, the space velocity of the feed gas (GHSV or WHSV) also has a significant effect on the reforming reaction. The pace velocity directly affects the amount of reaction products as well as the contact time between the feed gas and the catalyst. The dry reforming of methane is a solid type heterogeneous catalytic reaction. In this type of reaction, it is assumed that the gaseous molecules of methane and carbon dioxide are adsorbed on the surface of the catalyst, decomposed on the catalyst surface, and then undergo the main reforming reaction. Increasing the space velocity may slow down the adsorption of methane and carbon dioxide molecules on the surface of the catalyst, which is an undesirable occurrence for the reforming process [8, 17]. ass transfer

of reactants also plays an important role in the reforming process. If the mass transfer resistance is low, the reaction of the reactant can be directly attributed to the basic kinetics of the catalyst. Therefore, in order to reduce the mass transfer resistance, space velocity is necessary to determine the dependence of the reactants on the space velocity after reaching a steady state [8]. However, thermodynamics and kinetics of the DRM reaction are affected by the mass transfer resistances, whether internal or external mass transfer limitations of the reactants. According to the point, in order to eliminate the external mass transfer resistance, it is necessary to test different space velocities (GHSV or WHSV) to determine that the reactants have reached a steady state value, so that further changes in GHSV or WHSV had a no effects the reactants. Another thing to consider is contact time. Contact time plays an important role in the conversion of CO_2 and CH_4. If the contact time is long, CO_2 or CH_4 conversion will not be affected. The contact time is inversely related to the space velocity, meaning that the lower the GHSV or WHSV, the longer the contact time. In order to eliminate the internal mass transfer resistance, the catalyst particle size should be as small as possible, so that further reduction in size will not affect the conversions of the reactants. In general, a high GHSV or WHSV and a small amount of a catalyst with small particle size can minimize the amount of external and internal mass transfer limitations, and conversely, a small amount of GHSV or WHSV is expected to cause severe mass transfer limitations. However, many studies have reported that even at low GHSVs or WHSVs for catalysts such as Ni/Al_2O_3 or Ni/TiO_2, high amounts of equilibrium conversions can be achieved. However, it is not possible to calculate a specific GHSV or

WHSV to eliminate the effect of the mass transfer restriction, but the experimental amount of GHSV or WHSV for each type of catalysts must be determined by testing [8, 18]. To do this, the GHSV or WHSV or WHSV value must be reduced step by step and the equilibrium information obtained using experimental experiments. Whenever the equilibrium data do not change by decreasing GHSV or WHSV, it can be stated with great confidence that the effects of the external mass transfer resistance are minimized and only the kinetic and thermodynamic effects of reactions affect on equilibrium results and the mass transfer resistance no longer has much effect on equilibrium results. Therefore, the reaction has reached the steady state equilibrium conversion value and the reaction is in the steady state [4].

The aim of this work is the calculation of the equilibrium composition of the DRM reaction using reaction coordinate and the Lagrange method. First, the Gibbs energy was calculated by the direct method and second, the reaction constant was calculated and then reaction coordinate and the equilibrium composition was estimated by two methods, directly and using the Lagrange method. In the end, these values have been compared with an empirical equilibrium composition that obtained with the experimental reaction by using the Ni/Al_2O_3 catalyst. Another purpose of this work is to investigate and determine the necessary conditions to achieve the appropriate conditions for the experimental equilibrium conversion and the appropriate space velocity to achieve the maximum amount of the experimental equilibrium conversion and compare it with the results of thermodynamic calculations.

2. Experimental

2.1. Catalyst preparation

The Ni supported catalyst prepared by the sol-gel method in our previous work has been used for obtaining the equilibrium composition [19, 20]. The $Al(NO_3)_3.9H_2O$ used as the alumina precursor and citric acid were dissolved in distilled water separately. Then the citric acid solution was added to the alumina solution and stirred vigorously until a homogenized solution was prepared (solution 1). Then $Ni(NO_3)_2.6H_2O$ was added to the solution 1. The mixture was stirred vigorously for 5 h, and then that solution was kept at room temperature to obtain a uniform gel. That gel was dried at 383.15 K for 12 h and then calcined at 823.15 K for 6 h.

2.2. Catalyst characterization

The XRD test (Broker D8) was used for the indication of all phases in the catalyst structure. The FESEM/EDX (TSCANS) analysis was used for investigating the morphology of the catalyst structure and finding all elements in the samples.

2.3. Experimental test

The activity analysis was studied at atmospheric pressure and different temperatures ranged from 873.15 to 1173.15 K with different GHSVs ranged from 8400 to 14400 $ml.h^{-1}g^{-1}$. 50 mg of the catalyst with 250 mg of quartz with mesh 30-60 as an inert solid that was fixed in the quartz microreactor with internal diameter = 2 mm and length = 50 cm, were used for the activity test. The feed flow contains methane and carbon dioxide with a 1/1 molar ratio. Inlet and outlet gasses from microreactor were analyzed with online GC that was equipped with Propack Q and Molecular sieve columns and a TCD as a detector. Before the activity test, the catalyst was heated and reduced with the H_2 flow (30

ml/min) from room temperature to 973 K for 3 h and kept at that temperature for 1 h. After that, the sample was cooled with the H_2 flow to room temperature and then heated with the feed stream from that temperature to the reaction temperature after 3 h [20]. The schamitcs of the experimental setup are presented in Figure 1 [21].
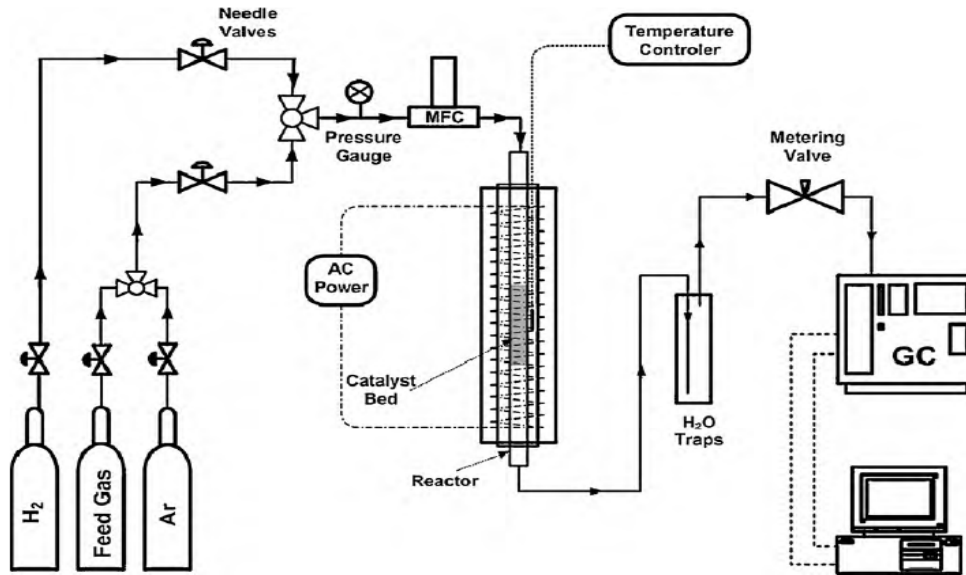

Figure 1. Schematic view of the experimental set up for the methane reforming.

3. Thermodynamic calculation

For determining the equilibrium composition, three states were considered. In the first state, reaction No. 1 was selected and the reaction constant was estimated via the free Gibbs energy, then reaction coordinate was calculated. For the second state, reaction No.1 and 2 were chosen and then the reaction constant, free Gibbs energy and reaction coordinate for those two reactions calculated. For the third state, all the reactions (No. 1-10) were selected and then all equations were solved to obtain equilibrium compositions. In the first state, CH_4, CO_2, CO and H_2 spices exist in the equilibrium system and for the second state, H_2O is added to the system. For these reactions, the direct method has been used for determining the equilibrium compositions.

Under the equilibrium condition, the rate of the change of the total Gibbs energy for the system was equal to zero. v_i was the

stoichiometric coefficient and μ_i, was a chemical potential for i_{th} spices in the reaction [15, 16].

$$\sum_i v_i \mu_i = 0 \tag{11}$$

So the fugacity of the component (i) in the system is as follows [15, 16]:

$$\mu_i = \Gamma_i(T) + RT \ln (\hat{f}_i) \tag{12}$$

For the component (i) in the pure state and under the standard condition the free Gibbs energy was calculated by [15, 16]:

$$G_i^0 = \Gamma_i(T) + RT \ln (\dot{f}_i) \tag{13}$$

The dfference between eqs.12 and 13 results:

$$\mu_i - G_i^0 = RT \ln \left(\frac{\hat{f}_i}{\dot{f}_i}\right) \tag{14}$$

With the combination of equations 11 and 14 and simplification of the obtained reaction, the relation (equation 16) between the reaction constant and fugacity for all components was achieved [15, 16].

$$\ln \prod_i (\frac{\hat{f}_i}{f_i})^{v_i} = \frac{\sum_i v_i G_i^0}{RT} \tag{15}$$

$$\prod_i (\frac{\hat{f}_i}{f_i})^{v_i} = K \tag{16}$$

So K, the reaction constant was calculated by [15, 16]

$$K = \exp(\frac{-\Delta G^0}{RT}) \tag{17}$$

In order to calculate the free Gibbs energy for reaction at any temperature, equation No. 18 was used [15, 16]

$$\frac{\Delta G^0}{RT} = \frac{\Delta G_0^0 - \Delta H_0^0}{RT_0} + \frac{\Delta H_0^0}{RT} + \frac{1}{T}\int_{T_0}^T \frac{\Delta C_P^0}{R} dt \tag{18}$$
$$- \int_{T_0}^T \frac{\Delta C_P^0}{R} \frac{dt}{T}$$

In the gas phase reaction, the fugacity of the ideal component under the standard condition was equal to pressure, so equation No. 16 became [15, 16]:

$$\prod_i (\frac{\hat{f}_i}{P^0})^{v_i} = K \tag{19}$$

When the expression eqivalent to fugacity is placed in eq.19, the following equation results [15, 16]:

$$\prod_i (\frac{\hat{\Phi}_i y_i P}{P^0})^{v_i} = K \tag{20}$$

In low pressures or high temperatures, the mixture acted as an ideal gas, so equation No. 20 became [15, 16]:

$$\prod_i (y_i)^{v_i} = K \left(\frac{P}{P^0}\right)^{-v_i} \tag{21}$$

For the first and second states, the mole fractions for all spices in the reaction were calculated from the below equation. In this equation, ε is the reaction coordinate. (i) is used for the pure species and (j) is used for the reaction number. Table 1 presents the stoichiometric coefficients for reactions No. 1 and 2 [15, 16].

$$y_i = \frac{n_{i_0} + \sum_j v_{i,j}\varepsilon_j}{n_0 + \sum_j v_j \varepsilon_j} \tag{22}$$

Table 1
The stoichiometric coefficients for reactions No. 1 and 2.

i	CH$_4$	CO$_2$	CO	H$_2$	H$_2$O	Reaction
j						v_j
1	-1	-1	2	2	0	2
2	0	-1	1	-1	1	0

So for calculating the mole fraction and reaction constant for the first state, equations No. 23-27 were used.

$$y_{CH_4} = \frac{1 - \varepsilon}{2 + 2\varepsilon} \tag{23}$$

$$y_{CO_2} = \frac{1 - \varepsilon}{2 + 2\varepsilon} \tag{24}$$

$$y_{co} = \frac{2\varepsilon}{2 + 2\varepsilon} \tag{25}$$

$$y_{H_2} = \frac{2\varepsilon}{2 + 2\varepsilon} \tag{26}$$

$$K = \frac{y_{co}^2 y_{H_2}^2}{y_{CO_2} y_{CH_4}} \tag{27}$$

For calculating the mole fraction and reaction constant for the second state, equations No. 28-34 were used.

$$y_{CH_4} = \frac{1 - \varepsilon_1}{2 + 2\varepsilon_1} \tag{28}$$

$$y_{CO_2} = \frac{1 - \varepsilon_1 - \varepsilon_2}{2 + 2\varepsilon_1} \tag{29}$$

$$y_{co} = \frac{2\varepsilon_1 + \varepsilon_2}{2 + 2\varepsilon_1} \tag{30}$$

$$y_{H_2} = \frac{2\varepsilon_1 - \varepsilon_2}{2 + 2\varepsilon_1} \tag{31}$$

$$y_{H_2O} = \frac{\varepsilon_2}{2 + 2\varepsilon_1} \tag{32}$$

$$K_1 = \frac{y_{co}{}^2 y_{H_2}{}^2}{y_{CO_2} y_{CH_4}} \tag{33}$$

$$K_2 = \frac{y_{co} y_{H_2o}}{y_{CO_2} y_{H_2}} \tag{34}$$

In the third state, the Lagrange method was used for calculating the mole fraction. It was difficult to use the direct method, when all reactions were selected, to calculate the mole fraction. In this method without considering the number of reactions, the mole fractions of all species are calculated by the below equation [15]:

$$\frac{\Delta G_{fi}^0}{RT} + \ln y_i + \sum_i \frac{\lambda_k}{RT} a_{ik} = 0 \tag{35}$$

In this reaction, ΔG_{fi}^0, is the free Gibbs energy of the formation of the component (i) at the T temperature, y_i, is the mole fraction of spices (i), λ_k, is the Lagrange coefficient of the kth element and a_{ik}, is the total atomic masses for the kth element present in reactions. In the DRM reaction and by considering all reactions (1-10), there are five species. Table 2 shows the a_{ik}s of all species.

Table 2
a_{ik} of all elements present in the DRM for the third state.

Component	a_{ik}		
	H	**O**	**C**
CH_4	4	0	1
CO_2	0	2	1
CO	0	1	1
H_2	2	0	0
H_2O	2	1	0

For the calculation of the mole fraction by the Lagrange method, the equations No. 36-40 were used. In these equations, all the mole fractions and Lagrange coefficients are undefined and need to be calculated. There are nine undefined values so nine equations must be used for estimating these parameters.

$$\frac{\Delta\dot{G}_{fCH_4}}{RT} + \ln(y_{CH_4}) + \frac{\lambda_c}{RT} + 4\frac{\lambda_H}{RT} = 0 \tag{36}$$

$$\frac{\Delta\dot{G}_{fCO_2}}{RT} + \ln(y_{CO_2}) + \frac{\lambda_c}{RT} + 2\frac{\lambda_O}{RT} = 0 \tag{37}$$

$$\frac{\Delta\dot{G}_{fCO}}{RT} + \ln(y_{CO}) + \frac{\lambda_c}{RT} + \frac{\lambda_O}{RT} = 0 \tag{38}$$

$$0 + \ln(y_{H_2}) + 2\frac{\lambda_H}{RT} = 0 \tag{39}$$

$$\frac{\Delta\dot{G}_{fH_2O}}{RT} + \ln(y_{H_2O}) + \frac{\lambda_O}{RT} + 2\frac{\lambda_H}{RT} = 0 \tag{40}$$

The other three equations are the mass balance on each k species that is present in reaction.

$$C: y_{CH_4} + y_{CO} + y_{CO_2} = \text{initial element in}/n \tag{41}$$

$$H: 4y_{CH_4} + 2y_{H_2} + 2\,y_{H_2O} = \text{initial element in}/n \tag{42}$$

$$O: 2y_{CO_2} + y_{CO} + y_{H_2O} = \text{initial element in}/\,n \tag{43}$$

The last reaction was for the summation of mole fractions.

$$y_{CH_4} + y_{CO} + y_{CO_2} + y_{H_2} + y_{H_2O} = 1 \tag{44}$$

under all conditions, the CH_4/CO_2 ratio is equal to 1 and the initial concentration of this component is assumed to be 1 mol/lit. In all states and for the empirical equilibrium, the conversions are calculated by Eq. 45 as follows:

$$X_{component} = \frac{[C]_{initial} - [C]_{final}}{[C]_{initial}} \quad (45)$$

To compare these methods with the empirical equilibrium that was obtained by the activity test, the error factor has been defined by the following equation:

$$error = \frac{[X]_{empirical} - [X]_{theoretical}}{[X]_{empirical}} \quad (46)$$

4. Results and discussion

4.1. Characterization

The XRD pattern of Ni/Al_2O_3 shows two broad peaks between 24-50° and 50-67° that are arttibuted to the amorphous structure. There is no peak of $NiAl_2O_4$ in the XRD patterns of Ni/Al_2O_3. In fact, in the sol-gel preparation, there is the high dispersion of Ni particles on the support. As a result, the presence and amount of the $NiAl_2O_4$ spinel depend on the preparation method. Also there is no sign of NiO peaks in XRD patterns. The XRD patterns of this sample are presented in Figure 2. [20].

The FESEM micrograph and EDX result of the sample are presented in Figure 3. As it is seen in this figure, the catalyst has an amorphous structure [20].
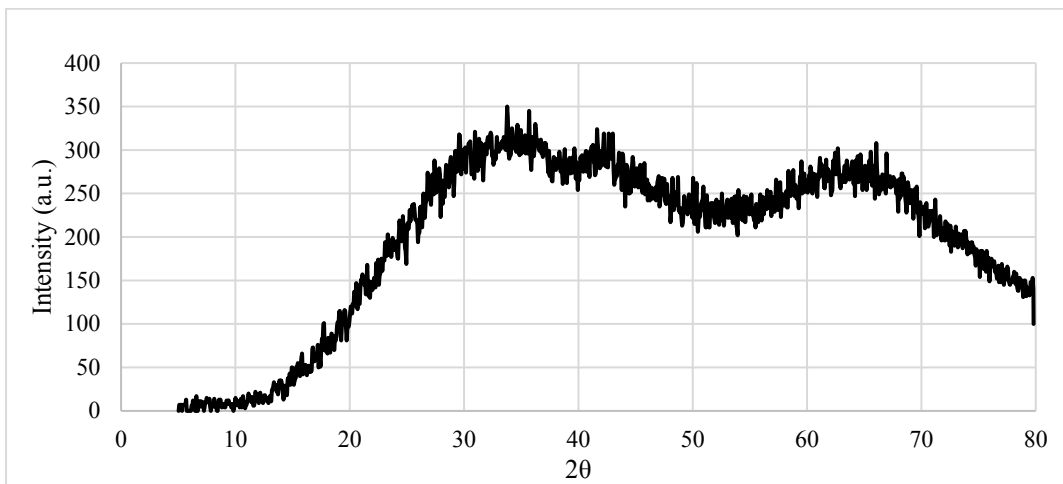
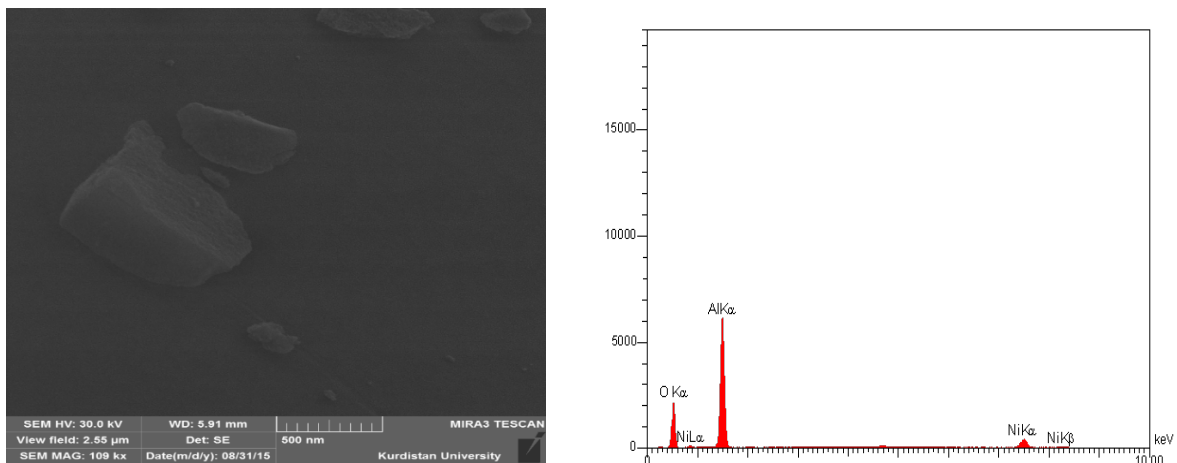

Figure 2. XRD pattern for Ni/Al_2O_3.

**Figure 3.** FESEM/EDX result for Ni/Al_2O_3.

4.2. Empirical equilibrium calculations

The effect of the GHSV on the methane and CO_2 conversions, and the H_2/CO ratio is shown in Figure 4 and Table 3. As it is seen in the figure and table, the methane and CO_2 conversions are increased by decreasing the GHSV. The gas velocity increases by increasing the GHSV and the mass transfer in the reaction, is improved in this situation. The contact time between gasses and catalyst solids decreased by increasing the GHSV. The methane and CO_2 conversion increases by decreasing the GHSV until these parameters reach a maximum value and show no more increase by decreasing the GHSV. It seems

that the mass transfer driving force under these conditions is equal to zero. Only under equilibrium conditions, the driving force of the mass transfer was equal to zero, so it seemed that the outlet gasses from the reaction reached the thermodynamic equilibrium. So in the end, this situation is called the empirical equilibrium [22].

The empirical equilibrium conversion and H_2/CO ratio are presented in Table 4. As mentioned above, conversions and the H_2/CO ratio increased by decreasing the GHSV at constant temperatures. And also, these parameters increase by increasing temperature at constant GHSVs.
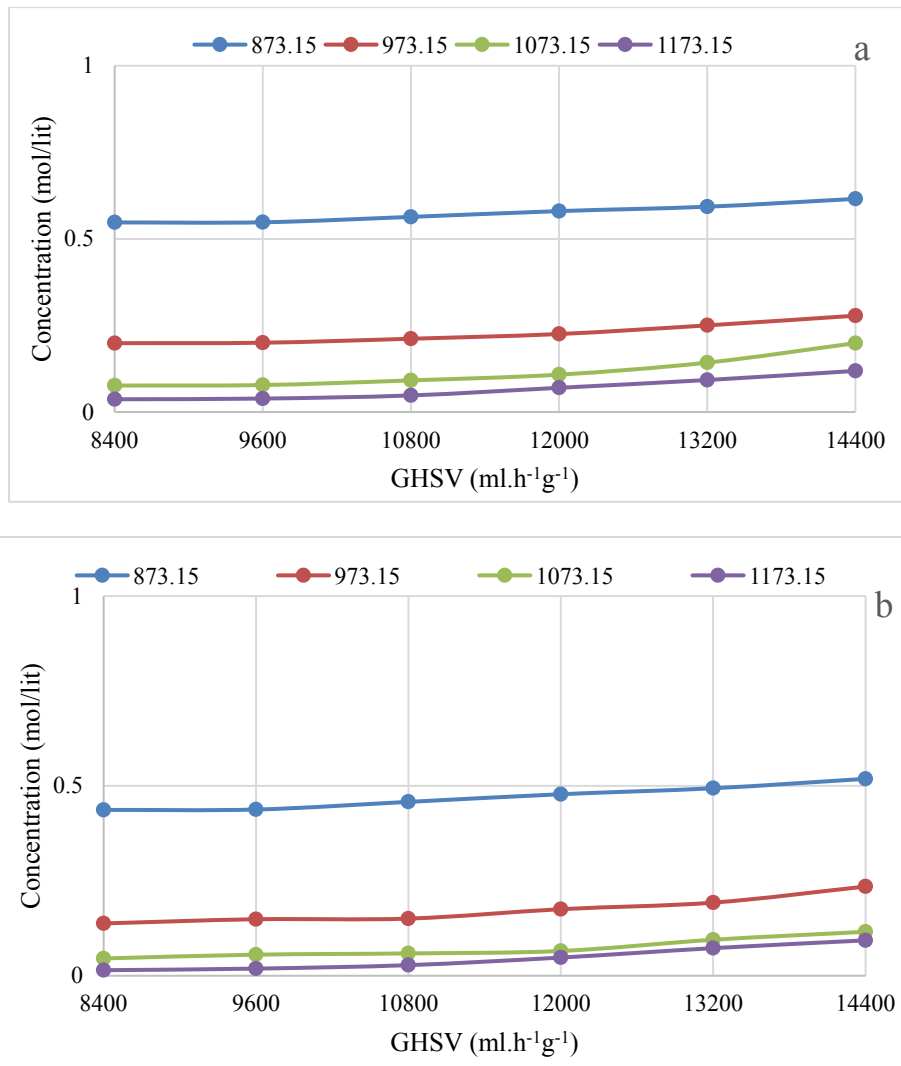
Figure 4. Results of the empirical equilibrium (a) Methane, (b) CO2 concentration vs. the GHSV at any temperature.

Table 3

Result for the empirical equilibrium.

| GHSV (ml.h⁻¹g⁻¹) | CH_4 concentration (mol/lit) | | | | CO_2 conversion (mol/lit) | | | |
| | T (K) | | | | T (K) | | | |
	873.15	973.15	1073.15	1173.15	873.15	973.15	1073.15	1173.15
14400	0.615	0.278	0.198	0.118	0.518	0.234	0.115	0.093
13200	0.592	0.25	0.142	0.092	0.493	0.192	0.094	0.072
12000	0.58	0.225	0.107	0.069	0.478	0.175	0.065	0.047
10800	0.563	0.211	0.091	0.047	0.453	0.150	0.058	0.027
9600	0.547	0.2	0.077	0.038	0.437	0.148	0.05	0.018
8400	0.547	0.198	0.076	0.036	0.436	0.137	0.0455	0.014

Table 4

Conversions and H_2/CO ratio for the empirical equilibrium.

| Parameter | T (K) | GHSV (ml.h⁻¹g⁻¹) | | | | | |
		14400	13200	12000	10800	9600	8400
CH₄ conversion (%)	873.15	38.45	40.71	41.98	43.65	45.21	45.25
	973.15	72.19	74.98	77.48	78.84	79.99	80.12
	1073.15	80.12	85.74	89.21	90.87	92.21	92.36
	1173.15	88.13	90.76	93.01	95.21	96.12	96.32
CO₂ conversion (%)	873.15	48.14	52.62	52.19	54.21	56.22	56.32
	973.15	76.51	80.74	82.47	84.95	85.12	86.21
	1073.15	88.42	90.52	93.48	94.12	94.45	95.45
	1173.15	90.68	92.73	95.21	97.21	98.12	98.54
H₂/CO	873.15	0.70	0.71	0.72	0.73	0.74	0.75
	973.15	0.85	0.86	0.87	0.88	0.89	0.90
	1073.15	0.91	0.92	0.93	0.94	0.945	0.95
	1173.15	0.95	0.96	0.97	0.981	0.985	0.99

4.3. Theoretical equilibrium calculations

By using equation No. 18, the Gibbs free energies, for the reactions No. 1 and 2 and then, the reaction constant (K), were calculated. Table 5 presents ΔG^0 and K for these reactions.

Using equations No. 23-34, the reaction coordinate (ε), mole fraction (y_i) and equilibrium compositions for these two reactions are calculated. For the first state, using reaction No. 1 for calculating equilibrium conditions, results show in Table 6 and for the second state, using both reaction No. 1 and 2 for finding equilibrium compositions, results show in Table 7. The concentration of the component and mole

fraction for the first and second states are demonstrated in Figures 5 and 6.

As it is seen in Figure 5 and Table 6, the mole fraction and concentration of reactants have the same value and for products also, these parameters have the same value.

Table 5

The ΔG^0 and reaction constant of reactions No. 1 and 2.

T (K)	ΔG^0(kJ/mol)		K	
	Reaction 1	**Reaction 2**	**Reaction 1**	**Reaction 2**
773.15	40.92	12.93	0.001	0.016
873.15	26.39	16.88	0.168	0.097
973.15	-15.09	7.9	6.458	0.376
1073.15	-43.08	-0.57	125.098	1.065
1173.15	71	-8.54	1454.428	2.400

Table 6

Result for reaction No. 1 (the first state).

T (K)	Mole fraction (%)					Concentration (mol/lit)					n
	CH_4	CO_2	CO	H_2	H_2O	CH_4	CO_2	CO	H_2	H_2O	(mol)
298.15	0.5	0.5	0	0	0	1	1	0	0	0	2
773.15	0.347	0.255	0.244	0.06	0.092	0.82	0.602	0.577	0.142	0.217	2.35
873.15	0.183	0.139	0.360	0.272	0.043	0.536	0.408	1.055	0.798	0.128	2.926
973.15	0.056	0.032	0.467	0.419	0.024	0.203	0.117	1.679	1.506	0.086	3.593
1073.15	0.021	0.011	0.488	0.468	0.009	0.081	0.043	1.874	1.799	0.037	3.836
1173.15	0.005	0.002	0.497	0.49	0.003	0.023	0.009	1.967	1.939	0.014	3.953

Table 7

Result for reactions No. 1 and 2 (the second state).

| T (K)	ε_1	ε_2	Mole fraction (%)					Concentration (mol/lit)					n
			CH_4	CO_2	H_2	CO	H_2O	CH_4	CO_2	H_2	CO	H_2O	(mol)
298.15	0	0	0.5	0.5	0	0	0	1	1	0	0	0	2
773.15	0.1	0.08	0.409	0.372	0.127	0.054	0.036	0.9	0.82	0.28	0.12	0.08	2.2
873.15	0.4	0.07	0.214	0.189	0.310	0.26	0.025	0.6	0.53	0.87	0.73	0.07	2.8
973.15	0.72	0.06	0.081	0.063	0.436	0.401	0.017	0.28	0.22	1.5	1.38	0.06	3.44
1073.15	0.89	0.05	0.029	0.015	0.484	0.457	0.013	0.11	0.06	1.83	1.73	0.05	3.78
1173.15	0.95	0.03	0.012	0.005	0.494	0.479	0.007	0.05	0.02	1.93	1.87	0.03	3.9
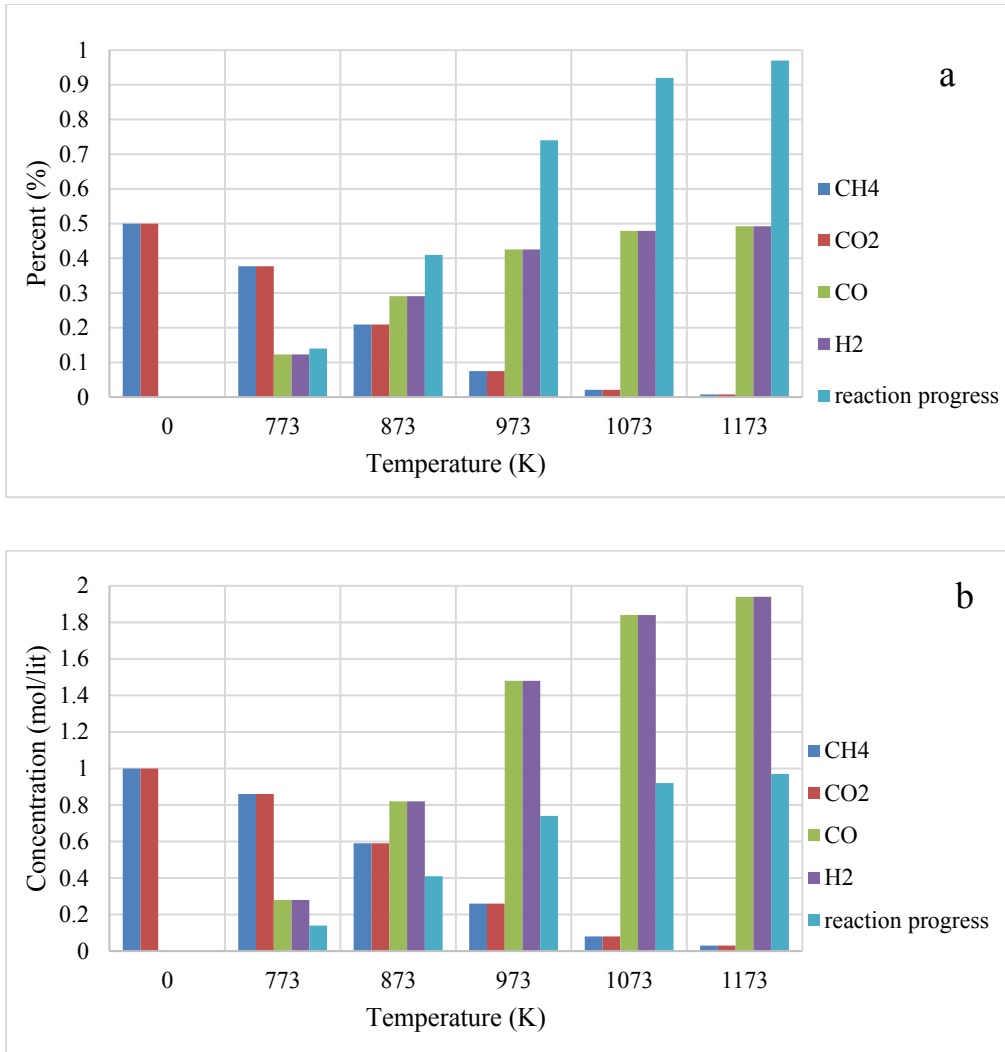
Figure 5. Mol fraction (a) and concentration (b) of all components for the first state.
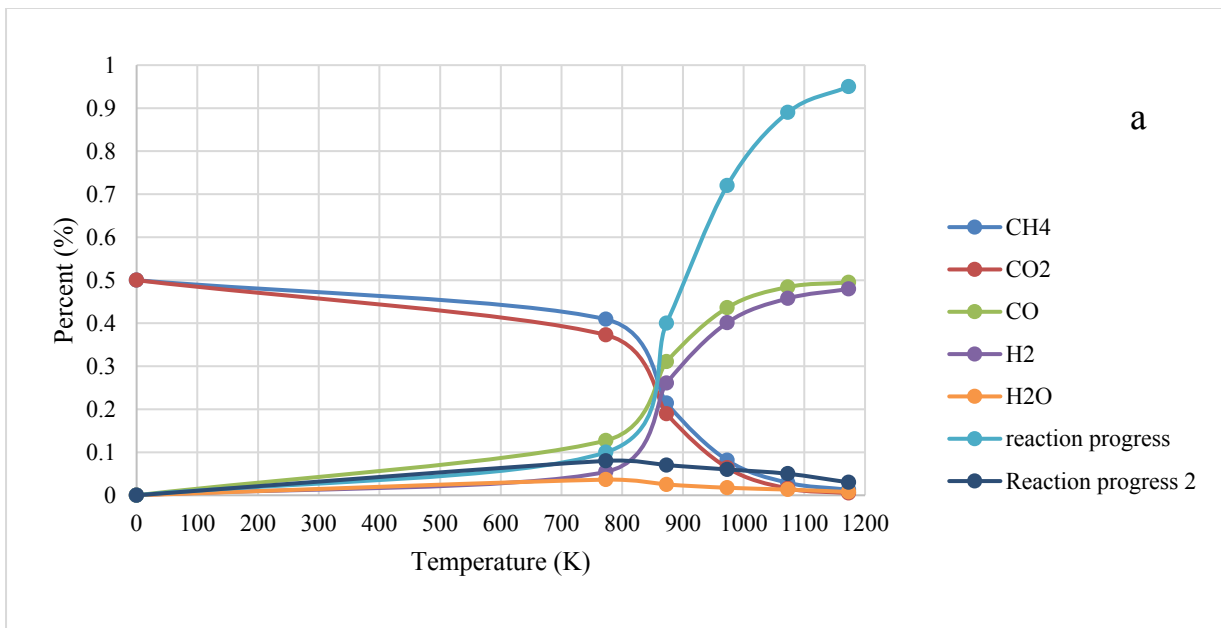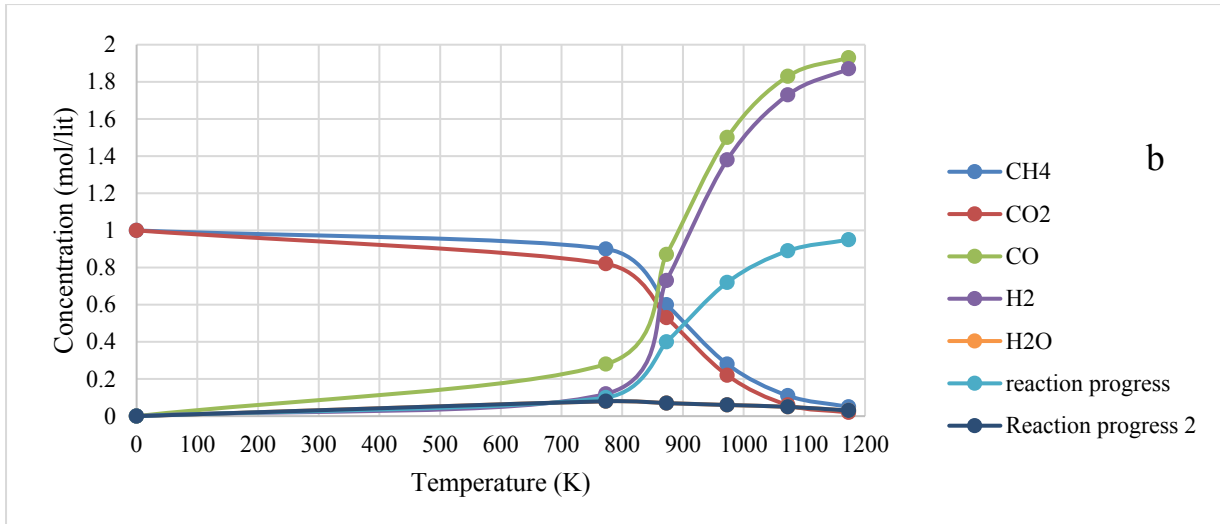
Figure 6. Mol fraction (a) and concentration (b) of all components for the second state.

As it is seen in Figure 6 and Table 7, the concentration and mole fraction of methane are higher than thoes of CO_2 and the concentration and mole fraction of H_2 are lower than thoes of CO. The RWGS reaction was the main reason of this matter. Because CO_2 and H_2 were consumed by the RWGS reaction, so the concentrations of the outlet CO_2 and H_2 were lower than the concentrations of methane and CO respectively.

For using the second method, the Lagrange

method, first ΔG_{fi}^0 for all samples must be calculated at different temperatures. This parameter is calculated by using equation No. 18 and ΔG_{fi}^0 is assumed zero for the pure element. The result is presented in Table 8. Then by using equations No. 36-44 the mole fraction and concentration of all components are calculated. In this situation, the reaction coordinate wasn't calculated. This result is also presented in Figure 7.

Table 8

ΔG_{fi}^0 (J/mol) for all materials at different Ts (K).

Component	773.15	873.15	973.15	1073.15	1173.15
CH_4	-5164.64	5466.04	16248.15	25248.39	38089.96
CO_2	-396011	-395605.22	-395689	-395763	-395824
CO	-182060	-191814.55	-201884	-208858	-219027
H_2O	-207918	-197246.71	-194320	-188791	-183203

Table 9

Result for reactions No. 1 and 2 (the second state).

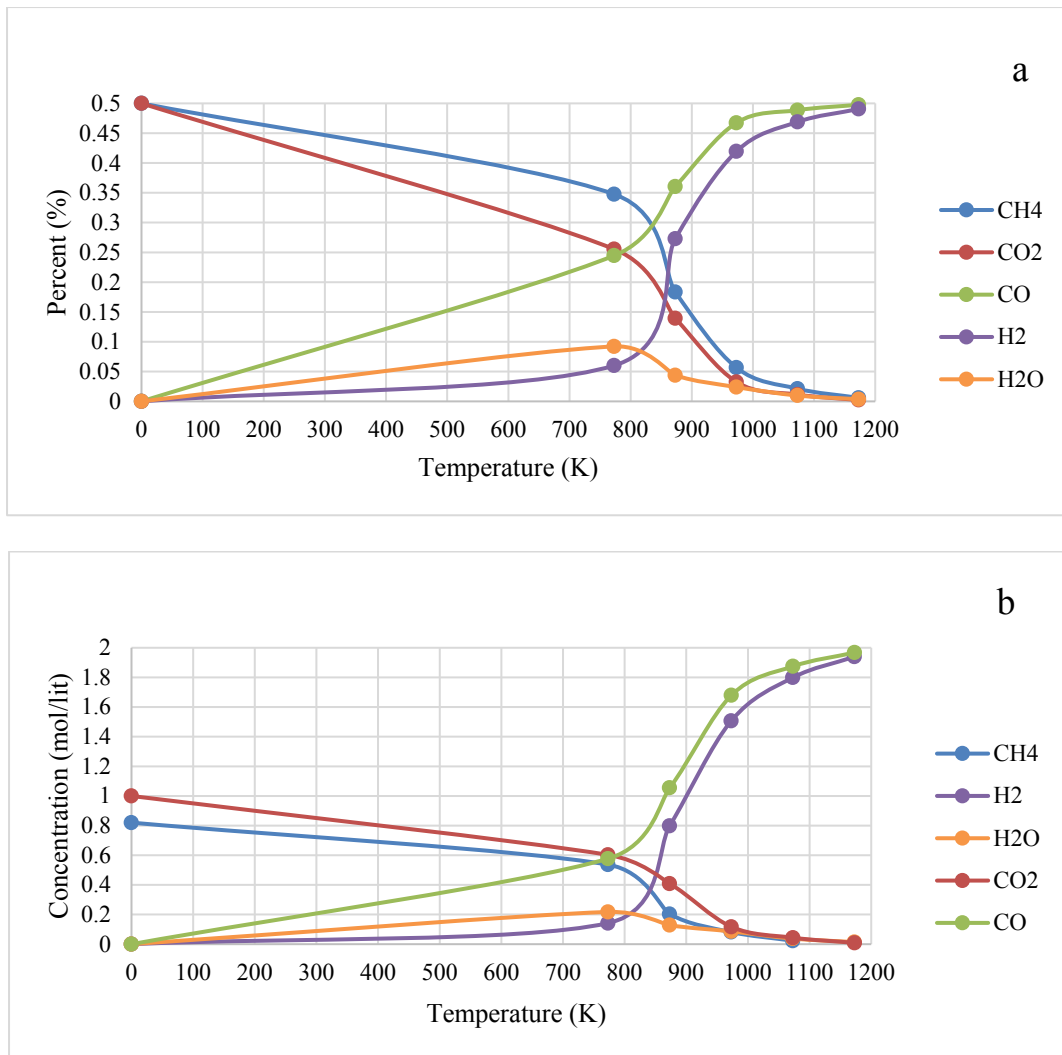| T (K)	Mole fraction (%)					Concentration (mol/lit)					n (mol)
	CH_4	CO_2	CO	H_2	H_2O	CH_4	CO_2	CO	H_2	H_2O	
298.15	0.5	0.5	0	0	0	1	1	0	0	0	2
773.15	0.347	0.255	0.244	0.06	0.092	0.82	0.602	0.577	0.142	0.217	2.35
873.15	0.183	0.139	0.360	0.272	0.043	0.536	0.408	1.055	0.798	0.128	2.926
973.15	0.056	0.032	0.467	0.419	0.024	0.203	0.117	1.679	1.506	0.086	3.593
1073.15	0.021	0.011	0.488	0.468	0.009	0.081	0.043	1.874	1.799	0.037	3.836
1173.15	0.005	0.002	0.497	0.49	0.003	0.023	0.009	1.967	1.939	0.014	3.953

Figure 7. Mole fraction (a) and concentration (b) of all components for the third state.

As it is seen in Figure 7 and Table 9, without considering the number of reactions that occurred in DRM, at all temperatures, the concentrations of methane, and the produced CO were higher than the concentrations of CO_2 and H_2. But the concentration of H_2O was decreased by increasing temperature.

As it is seen in all figures and tables, by increasing temperature, the concentrations and fractions of methane and CO_2 are decreased, and the concentrations of H_2 and CO are increased increasing temperature. Table 10 shows the equilibrium conversion and H_2/CO produced during DRM in all three states and empirical state.

So by comparing between these three theoretical states, methane and CO_2 conversion for the third state was higher than the other states. To choose the best method between these states for estimating equilibrium compositions, the result must be compared with empirical equilibrium. Empirical equilibrium occurred when GHSV = 8400 $ml.h^{-1}.g^{-1}$. The result presented in Table 10. None of these states can completely describe equilibrium compositions, but there was a good agreement between the third state and empirical equilibrium at all temperatures. The theoretical conversion had a good agreement with other research [4, 5, 10, 11, 14, 17]. Error factor for all state calculated with equation No. 47 presented in Table 11. As seen in this table,

at high temperature (above 1073.15 K), the error between theoretical and empirical value was less than $\pm 5\%$, so there wasn't any

significant difference between these three theoretical states and experimental condition.

Table 10

Conversion, and H_2/CO ratio from theoretical and empirical equilibrium.

T (K)	State 1			State 2			State 3			Empirical		
	x_{CH_4}	x_{CO_2}	$\frac{H_2}{CO}$	x_{CH_4}	x_{CO_2}	$\frac{H_2}{CO}$	x_{CH_4}	x_{CO_2}	$\frac{H_2}{CO}$	x_{CH_4}	x_{CO_2}	$\frac{H_2}{CO}$
298.15	0	0	-	0	0	-	0	0	-	0	0	0
773.15	14	14	1	10	18	0.42	17.98	39.73	0.24	-	-	-
873.15	41	41	1	40	47	0.83	46.32	59.17	0.75	45.25	56.32	0.75
973.15	74	74	1	72	78	0.92	79.66	88.28	0.89	80.12	86.215	0.90
1073.15	92	92	1	89	94	0.94	91.82	95.62	0.95	92.36	95.45	0.95
1173.15	97	97	1	95	98	0.96	97.66	99.09	0.98	96.32	98.54	0.99

Table 11

Error factor for conversion, and H_2/CO ratio.

T (K)	State 1-error			State 2-error			State 3-error		
	x_{CH_4}	x_{CO_2}	$\frac{H_2}{CO}$	x_{CH_4}	x_{CO_2}	$\frac{H_2}{CO}$	x_{CH_4}	x_{CO_2}	$\frac{H_2}{CO}$
873.15	0.093	0.27	-0.333	0.116	0.165	-0.106	-0.023	-0.0506	0
973.15	0.076	0.141	-0.111	0.101	0.095	-0.022	0.005	-0.023	0.011
1073.15	0.003	0.036	-0.052	0.036	0.015	0.010	0.005	-0.001	0
1173.15	-0.007	0.015	-0.010	0.013	0.005	0.030	-0.013	-0.0055	0.010

5. Conclusions

Equilibrium concentration from the theoretical method and empirical method for dry reforming of methane calculated in this paper. reaction coordinate and reaction constant are estimated by the minimization of the free Gibbs energy. The free Gibbs energy is calculated by the direct method and Lagrange method. The empirical equilibrium was measured by decreasing the GHSV of the feed flow at different temperatures till reaching the concentration of equilibrium compositions. Concentrations and conversions that were calculated by the Lagrange method and by using the free Gibbs energy of formation were in good agreement with an empirical equilibrium that was calculated by decreasing the GHSV of the feed flow on Ni/Al_2O_3 at any temperature. At high temperatures (above

1073.15 K) there was no significant difference between concentrations that were calculated by the direct method or Lagrange method and empirical equilibrium.

References

[1] Estephane, J., Aouad, S., Hany, S., El Khoury, B., Gennequin, C., El Zakhem, H., El Nakat, J., Aboukaïs, A. and Aad, E. A., "CO2 reforming of methane over Ni–Co/ZSM5 catalysts: Aging and carbon deposition study", *International Journal of Hydrogen Energy*, **40** (30), 9201 (2015).

[2] Majhi, S., Mohanty, P., Wang, H. and Pant, K., "Direct conversion of natural gas

to higher hydrocarbons: A review", *Journal of Energy Chemistry*, **22** (4), 543 (2013).

[3] Usman, M., Daud, W. and Abbas, H. F., "Dry reforming of methane: Influence of process parameters—A review", *Renewable and Sustainable Energy Reviews*, **45**, 710 (2015).

[4] Palmer, C., Upham, D. C., Smart, S., Gordon, M. J., Metiu, H. and McFarland, E. W., "Dry reforming of methane catalysed by molten metal alloys", *Nature Catalysis*, **3** (1), 83 (2020).

[5] Bach, V. R., de Camargo, A. C., de Souza, T. L., Cardozo-Filho, L. and Alves, H. J., "Dry reforming of methane over Ni/MgO–Al$_2$O$_3$ catalysts: thermodynamic equilibrium analysis and experimental application", *International Journal of Hydrogen Energy*, **45** (8), 5252 (2020).

[6] Gosiewski, K., "Mathematical simulations of reactors for catalytic conversion of methane to syngas with forced concentration cycling", *Chemical Engineering and Processing: Process Intensification*, **39** (5), 459 (2000).

[7] Hou, K. and Hughes, R., "The kinetics of methane steam reforming over a Ni/α-Al$_2$O$_3$ catalyst", *Chemical Engineering Journal*, **82** (1), 311 (2001).

[8] Pham, T. P., Ro, K. S., Chen, L., Mahajan, D., Siang, T. J., Ashik, U., Hayashi, J. -I., Minh, D. P. and Vo, D. -V. N., "Microwave-assisted dry reforming of methane for syngas production: A review", *Environmental Chemistry Letters*, 1 (2020).

[9] Chan, S. and Wang, H., "Thermodynamic analysis of natural-gas fuel processing for fuel cell applications", *International Journal of Hydrogen Energy*, **25** (5), 441 (2000).

[10] Lutz, A. E., Bradshaw, R. W., Keller, J. O. and Witmer, D. E., "Thermodynamic analysis of hydrogen production by steam reforming", *International Journal of Hydrogen Energy*, **28** (2), 159 (2003).

[11] Istadi, I., Amin, N. A. S. and Aishah, N., "Co-generation of C2 hydrocarbons and synthesis gases from methane and carbon dioxide: A thermodynamic analysis", *Journal of Natural Gas Chemistry*, **14** (3), 140 (2005).

[12] Douvartzides, S., Coutelieris, F., Demin, A. and Tsiakaras, P., "Fuel options for solid oxide fuel cells: A thermodynamic analysis", *AIChE Journal*, **49** (1), 248 (2003).

[13] Juan-Juan, J., Román-Martınez, M. and Illán-Gómez, M., "Catalytic activity and characterization of Ni/Al$_2$O$_3$ and NiK/Al$_2$O$_3$ catalysts for CO$_2$ methane reforming", *Applied Catalysis A: General*, **264** (2), 169 (2004).

[14] Wolf, M., "Thermodynamic assessment of the stability of bulk and nanoparticulate cobalt and nickel during dry and steam reforming of methane", *RSC Advances*, **11** (30), 18187 (2021).

[15] Abbott, M. M., Smith, J. M. and Van Ness, H. C., Introduction to chemical engineering thermodynamics, 8th Ed., McGraw-Hill, New York, USA, p. 559 (2018).

[16] Ahuja, P., Chemical engineering thermodynamics, 1st Ed., PHI Learning Pvt. Ltd, (2008).

[17] Xia, Y., Wang, S., Shi, C., Xu, J., Xia, R., Xu, H. and Xing, S., "Research progress of thermodynamic simulation for methane dry reforming", *Academic Journal of Engineering and Technology Science*, **3** (1), 101 (2020).

[18] Abdullah, B., Abd Ghani, N. A. and Vo,

D. -V. N., "Recent advances in dry reforming of methane over Ni-based catalysts", *Journal of Cleaner Production*, **162,** 170 (2017).

[19] Sharifi, M., Haghighi, M., Rahmani, F. and Rahemi, N., "Reforming of biogas over Co-and Cu-promoted Ni/Al$_2$O$_3$-ZrO$_2$ nanocatalysts synthesized via sequential impregnation method", *Journal of Renewable Energy and Environment*, **1** (1), 53 (2014).

[20] Moradi, Gh., Khezeli, F. and Hemmati, H., "Syngas production with dry reforming of methane over Ni/ZSM-5 catalysts", *Journal of Natural Gas Science and Engineering*, **33**, 657 (2016).

[21] Moradi, Gh., Hemmati, H. and Rahmanzadeh, M., "Preparation of a LaNiO$_3$/γ-Al$_2$O$_3$ catalyst and its performance in dry reforming of methane", *Chemical Engineering & Technology*, **36** (4), 575 (2013).

[22] Moradi, Gh., Ahmadpour, J., Nazari, M. and Yaripour, F., "Effects of feed composition and space velocity on direct synthesis of dimethyl ether from syngas", *Industrial & Engineering Chemistry Research*, **47** (20), 7672 (2008).